ASTRONOMY & ASTROPHYSICS
SUPPLEMENT SERIES

Astron. Astrophys. Suppl. Ser. **61**, 141-162 (1985)

Luminosity and mass models for the barred spiral galaxies NGC 7741, NGC 3359 and NGC 7479 (*)

M. F. Duval [1] and G. Monnet [2]

[1] Observatoire de Marseille, 2, place Le Verrier, 13248 Marseille Cedex 4, France
[2] Observatoire de Lyon, 69230 Saint-Genis-Laval, France

Received October 11, 1984, accepted March 1, 1985

Summary. — Luminosity distributions and mass models of three barred spiral galaxies have been obtained from two-dimensional photometric data and the radial velocity field of the ionized gas.
The « S » shaped distortion due to the gravitational pull of the bar appears clearly. The blue M/L ratios of the bars are quite comparable to those of the disks at the same radii ($M/L \sim 4$).

Key words : barred galaxies — kinematics and dynamics of galaxies.

1. Introduction.

We have studied three late type barred spirals [1], NGC 7741, NGC 3359, and NGC 7479, in a similar way to NGC 5383 (Duval and Athanassoula, 1983, hereafter referred to as Paper I). From photographic surface photometry, we have built luminosity models with several components (Sect. 2). The radial velocity field of the ionized gas from long slit spectroscopy is given in section 3, and used to derive mass models. Conclusions are given in section 4.

2. Luminosity models.

2.1 Observations and reductions. — Blue plates were obtained at the F/6 Focus (scale 28″6 mm^{-1}) of the 120 cm telescope at Haute Provence Observatory. The best plate for each galaxy (respectively numbered L 2377, L 2469, L 2557) was reduced as explained in Paper I. Absolute values were obtained by using photoelectric aperture photometry as follows : for NGC 7741, by de Vaucouleurs G. and A. (1972), Holmberg (1958), Bigay *et al.* (1953) and Pettit (1954) (some Pettit discrepant values were excluded and complementary values published by Longo and A. de Vaucouleurs, 1983, unknown at that time) we found a night sky background $\mu_s = 22.00$ mag arcsec^{-2}; for NGC 3359, by Pettit (1954) and Holmberg (1958), there are rather few and old data, however, they lead to a reasonable night-sky background of $\mu_s = 21.60$ mag arcsec^{-2}; and for NGC 7479, by Benedict (1982), de Vaucouleurs, G. and A. (1972), Pettit (1954), Stebbins and Whitford (1937) (Tifft, 1963 data were excluded), the night sky background is $\mu_s = 21.53$ mag arcsec^{-2}.

The resulting blue isophotal maps are presented in figures 1a, b and c. Figures 2a, b and c show the equivalent mean luminosity profiles and the relative integrated luminosity curves.

The photometric values are given in tables Ia, b and c, where according to de Vaucouleurs' (1962) precepts, we give :

Column 1 : log I, where I is the luminosity for a given isophote in units of the night-sky background.
Column 2 : μ_B = corresponding luminosity in magnitude arcsec^{-2}.
Column 3 : $\mathcal{A}$ = area in square minutes enclosed within the isophote.
Column 4 : r^* = equivalent radius in minutes $(=\sqrt{\mathcal{A}/\pi})$.
Column 5 : $L(r^*)$ = integrated luminosity out to r^* in units of $I \times$ square minutes.
Column 6 : $k(r^*) = L(r^*)/L_T$ fraction of the total luminosity interior to r^*.
Column 7 : log ρ^*, where $\rho^* = r^*/r^*_e$ is the equivalent radius normalized to the effective equivalent radius.
Column 8 : $m(\rho^*)$ = integrated magnitude out to ρ^*.

The total apparent magnitudes B_T derived from extrapolation of the mean luminosity profiles and the B^o_T magnitudes corrected from galactic and internal absorption according to the RC2 (1976) values are given in table II

(*) The observations were made at the Observatoire de Haute Provence (CNRS).

Send offprint request to : M. F. Duval.

[1] This work is part of the 1984 « Thèse de Doctorat » at the Aix-Marseille I University by M. F. Duval, entitled « Aspects photométriques cinématiques et dynamiques de quelques galaxies barrées ».

so as the distance moduli found by Bottinelli *et al.* (1984) (which leads to a Hubble constant $H \simeq 100$ km s^{-1} Mpc^{-1}), and the absolute total luminosities.

2.2 LUMINOSITY MODELS. — Three components have been recognized in each galaxy and extracted through an iterative scheme similar to that used in Paper I. These are;

1) an extended exponential disk, of apparent axial ratio q_a, apparent central luminosity I'_o and equivalent radius a_e. Assuming an intrinsic axial ratio $q = 0.13$ for the Scd galaxy NGC 7741 and $q = 0.15$ for the Sc galaxies NGC 3359 and NGC 7479 (Bottinelli *et al.*, 1980), q_a is used to derive the inclination i of the galaxies ($i = 0°$, face on);

2) a central disk, with rather shape edges, and approximatively axisymmetric. Its luminosity I' along the line of sight is modelled by :

$$I' = I'_o\left(1 - \frac{a^2}{a_o^2}\right)^{\frac{n+1}{2}}$$

where I'_o is the apparent central luminosity, a the radius in the galaxy plane and a_o the outer radius of the central disk;

3) a prolate bar of semi-major axis a'_o at an angle θ'_o with the line of nodes in the sky plane, and with an observed ratio q_a. The true a_o, θ_o, q in the galaxy plane are computed with the classical formulae :

$$\text{tg}\,\theta_o = \text{tg}\,\theta'_o/\cos i\,, \quad a_o = a'_o \cos\theta'_o/\cos\theta_o$$
$$1 - q^2 = (1 - q_a^2)/(1 - q_a^2 \sin^2\theta_o \sin^2 i)\,.$$

The line of sight luminosity I' along the major axis is modelled by :

$$I' = I'_o\left(1 - \frac{a^2}{a_o^2}\right)^{\frac{n+1}{2}}.$$

The observed and derived parameters are given in table II.

No central bulges are observed for NGC 7741 and NGC 3359, to a level of at most 1 % of the total luminosity for the former, possibly larger for the latter but anyway hidden under the bright light of the central H II regions. There is a clearly discernable central bulge in NGC 7479. It fits a de Vaucouleurs $r^{1/4}$ law, with a central brightness $\mu_0 = 14.63$ mag arcsec^{-2} and an equivalent semi-major axis $a_e = 0'.29$. The agreement between the sum of the contributions of the modelled components and the mean luminosity profiles is shown in figures 2a, b, and c. As can be seen, an extra contribution is needed, which comes from the spiral arms and is especially important for NGC 3359.

Total relative luminosities L/L_T for each component are given in table III. It must be kept in mind that this scheme is somewhat over-simplified. There are some deviations, namely :

— warps in the central disk of NGC 7741 and the extended disk of NGC 7479

— some asymmetry of the central disks, especially that of NGC 3359

— significant off-centering of the bars of NGC 7741 and NGC 3359 (by respectively 7″ and 8″) from the extended isophotes centers, a common phenomenon for late-type barred spirals (de Vaucouleurs and Freeman, 1972).

2.3 DISCUSSION. — Good fits to both the mean and local luminosity distributions are obtained with the simple model chosen. We do not claim, however. that the division of the axisymmetric component between an exponential disk and a bell-shaped central disk — somewhat similar to a lens, but not aligned along the bar major axis — is necessarily physical. The luminosity data are generally in good agreement with other works, especially the detailed studies on NGC 7479 (Okamura, 1978; Benedict, 1982; Blackman, 1983). Different definitions of the components, however, explain the large differences in the relative contributions found by these authors.

The density law ($n = 0$ index) found for the bar of NGC 7479, a region of mild star formation, appears quite normal. On the other hand, NGC 7741 and NGC 3359 both exhibit highly centrally condensed bars, with respective indices of $n = 6$ and $n = 8$. This is clearly due to a contamination from very active star formation. Use of the least contaminated regions (East region between 20″ and 35″ for NGC 7741, South region for NGC 3359) suggests normal $n = 0$ laws for the old star component only. With the same semi-major ratios and apparent axial ratio, new line of sight luminosities are $I'^*_o = 22.2$ mag arcsec^{-2} for NGC 7741 and $I'^*_o = 22.6$ mag arcsec^{-2} for NGC 3359.

3. Kinematics and mass models.

3.1 OBSERVATIONS. — Radial velocities for the ionized gas were measured from image tube spectra taken with the Baranne-Pellet long slit spectrograph at the 193 cm OHP telescope (see Paper I for technical details and references). We reduced six spectra for NGC 7741, five for NGC 3359, and seven for NGC 7779. For NGC 7741 these results were complemented for the disks by two Fabry-Perot interferograms (BTA 23 and 24) taken at the 6 m — Zelenchuskaya telescope, with an interference order of 1360 at Hα.

3.2 RADIAL VELOCITY FIELDS. — The radial velocities, relative to the Sun, are given in tables IVa, b, and c. Mean radial velocities *versus* radius curves from spectra close (and parallel) to the major axis of the bars are shown in figures 3a, b, and c. They clearly show zones of small radial motions in the central part, out to $\simeq 1/2$ of the semi-major axis of the bar in the three objects, even in NGC 7479 with its non negligible bulge (which should in principle give a rather sharp velocity gradient). They also show, in the two galaxies with vigorous star formation (NGC 7741 and NGC 3359), a sharp bump just at the end of the bar. These two phenomena were also present in NGC 5383 (Paper I) where they were quantitatively identified with the perturbation of the gas flow by the asymmetric potential of the bar. The systematic velocities measured at the center of the galaxy are respectively :

$$V_S = 755 \text{ km s}^{-1} \text{ (NGC 7741)},$$
$$1000 \text{ km s}^{-1} \text{ (NGC 3359)}, \quad 2385 \text{ km s}^{-1} \text{ (NGC 7479)},$$

in good agreement with previous data (Sandage and Tammann, 1981).

3.3 AXISYMMETRIC MASS MODEL. — The velocity field is highly non-circular in the bar region, so the usual concept of a mean rotation curve has in principle no meaning. As shown in the Appendix (§ 1), if we admit a linear perturbation of the velocity field due to the bar, the axisymmetric rotation curve $U_{\theta,0}(\rho)$ can be derived from a Fourier-like transform of the radial velocity field $V_p(\rho)$, where ρ is the radius in the galaxy plane and $V_p = V_R - V_S$.

Specifically, if θ_0 is the angle between the bar and the line of nodes and i the inclination :

$$U_{\theta,0}(\rho) = \frac{2}{\pi \sin i \sin 2\,\theta_0} \int_{-\frac{\pi}{2}}^{+\frac{\pi}{2}} V_p(\rho) \sin(2\,\theta_0 - \theta)\, d\theta$$

(Eq. (4) of Appendix)

where θ is the azimuthal angle in the galaxy plane ($\theta = 0°$: major axis). The even non axisymmetric terms cancel in the integration over a half galaxy plane. (Odd terms, i.e. the effect of an off-centered bar, would cancel if the integration is carried over the whole plane, but we have not enough data even in the best case of NGC 7741.)

It has proved possible to apply this procedure only to NGC 7741, as the data on the other galaxies are too incomplete.

For that galaxy, we used the isoradial velocities in the galaxy half-plane as shown in figure 4.

For NGC 3359 and NGC 7479 we have, rather crudely, used the radial velocities near the line of nodes as a good approximation of the axisymmetric rotation field. For justification, see the Appendix (§ 1) and note the fair agreement between the axisymmetric curve obtained for NGC 7741 by the more rigorous method outlined above and the observed radial velocities near its line of nodes (Fig. 5a).

The rotation velocities are given in figures 5a, b and c.

The solid lines on the figures represent the axisymmetric rotation curves. They have been fitted by a sum of two Kuz'min-Toomre thin disk models (Kuz'min, 1953, Toomre, 1963).

A summation over Kuz'min-Toomre disks gives an angular velocity Ω such as :

$$\Omega^2 = \sum U_{\theta,0}^2/\rho^2 = \sum \frac{A}{(a^2 + \rho^2)^{3/2}}.$$

The A and a values are given in table V.

The mass of a disk integrated from the center to $\rho = ka$ is :

$$M(ka) = \frac{A}{G}\left[1 - \frac{1}{\sqrt{1 + k^2}}\right]$$

and the mass, in solar units, for a sum of two disks is :

$$M = 6.73 \times 10^4\, d \sum A\left[1 - \frac{1}{\sqrt{1 + k^2}}\right]$$

where d is the distance of the galaxy in Mpc.

The masses integrated from the center to the radius of the bar a_B are given in table V as the corresponding apparent luminosities. $L(a_B)$ is the sum of the total luminosity of the bar $L_{T,B}$ and of the luminosity of the axisymmetric components (central-disk, extended-disk, bulge for NGC 7479) up to a_B.

We give then the apparent mean M/L ratios over the same region.

3.4 MASS OF THE BAR. — The isoradial velocities (Figs. 6a, b, and c) clearly exhibit the classical « S » shaped distortion, expected from the gravitational pull of the bar. As shown in the Appendix (§ 2) we can use the observed radial velocities V_p at the end of the bar and the computed rotational velocity at radius a_B to find the normalizing coefficient $\lambda_B = f_B\, I'_{oB}\, q_{aB}\, r_B$ in km^2 s^{-2} (Eq. (5) of the Appendix). This coefficient is given in table VI.

With the photometric values I'_{oB}, q_{aB}, r_B and the distance moduli given in table II, we can calculate the Mass/Luminosity ratios $(M/L)_B = f_B = \lambda_B/0.0172\, I'_{oB}\, q_{aB}\, a_B$ (Table VI).

The very low values for NGC 7741 and NGC 3359 are due to the very active star formation in the bar. More meaningful values [$(M/L)^*$, Table VI] are obtained by referring only to the old stellar component of the bars (Sect. 2.4).

These values are very close for the three galaxies (and would be even closer if we could correct the luminosity of the bar of NGC 7479 for the faint, but present, star formation). They can be directly compared to the $(M/L)_a$ (Table VI) for the axisymmetric components, out to the same radius a_B computed from the (M/L) obtained in section 3.3 after removal of the contribution of the bar.

We see the near equality of the (M/L) ratios of the stellar bar and its surrounding disk for the first two galaxies, but a significantly lower value for NGC 7479. We recall that these values correspond to $H = 100$ km s^{-1} Mpc^{-1} (M/L ratios are $\propto h^{-1}$ with $h = 100/H$).

3.5 DISCUSSION. — The masses of the bars were obtained under two hypotheses, that the perturbation from the bar is linear and that corotation occurs at the end of the bar. We test the first hypothesis by computing the maximum perturbation of the largest Fourier component ϕ_2 of the potential. It is equal to $\simeq 0.43$ for an homogeneous bar of axial ratio $q = 0.25$ in Monnet-Simien (1977) units, and is attained at $\simeq 0.6$ (in unit of a_B).

$\Delta\phi_2$ in km^2 s^{-1} is equal to $0.43\,\lambda_B$, which gives respectively 1669, 1622, 2999 km^2 s^{-2} for the three galaxies. For a sum of Kuz'min-Toomre disks, the axisymmetric potential is given by $\phi_2 = \sum \frac{A}{\sqrt{a^2 + \rho^2}}$.

We obtain $\phi_2 = 27120$, 87400, 199400 km^2 s^{-2} for the 0.6 a_B radii (respectively 0'.44, 0'.38, 0'.56) and the ratios

$$\frac{\Delta\phi_2}{\phi_2} \text{ are : } 6 \times 10^{-2},\quad 2 \times 10^{-2},$$

and 1.5×10^{-2}, respectively.

This linear analysis appears thus quite justified.

The corotation hypothesis can be tested with the help of the familiar resonance curves Ω, $\Omega - \frac{\kappa}{2}$, $\Omega + \frac{\kappa}{2}$ as functions of radius, computed from the axisymmetric rotation curves (Sect. 3.3) by :

$$\Omega^2 = \sum \frac{A}{(a^2 + \rho^2)^{3/2}} \quad \kappa^2 = \sum \frac{A(4\,a^2 + \rho^2)}{(a^2 + \rho^2)^{5/2}}.$$

They are given in figures 7a, b, and c. For NGC 7741, the most exterior H II region is at $\simeq 135''$ (6.9 kpc) slightly outside the extent of the $\Omega + \frac{\kappa}{2}$ curve, but quite compatible in view of the uncertainties; however, the dust arms, on blue plates, are located on the inside of the blue stellar arms, while just the opposite is expected outside corotation. We have thus repeated the computation of the mass of the bar, putting corotation at $\simeq 108''$, which is the mean radius of a ring of H II regions. The result is essentially unchanged (the mass is only $\simeq 20\,\%$ larger).

For NGC 3359, the most exterior H II region is at $\simeq 210''$ (13 kpc) well outside the $\Omega + \frac{\kappa}{2}$ limit. Again, putting corotation further does not change the mass of the bar.

For NGC 7479, it is at $\simeq 225''$ (24.9 kpc) significantly outside the $\Omega + \frac{\kappa}{2}$ limit (even for a flat rotation curve, for $\rho > 120''$, the $\Omega + \frac{\kappa}{2}$ curve will cross Ω_p at $\rho = 150''$ only).

The influence on the mass of the bar is again small.

We thus see in the three cases significant evidence against theoretical expectations, but rather negligible influence on the derived M/L ratios of the bars.

4. Conclusions.

The « incorruptible S shaped distortion » in the isovelocities of the gas in a barred galaxy, predicted by Kalnajs (1978), was first noticed by Bosma (1978) from H I supersyntheses data on spirals and optically by Peterson *et al.* (1978) on the « prototype » object, NGC 5383. Since then, it has been confirmed, more or less, for a number of barred galaxies : NGC 1300 (Peterson and Huntley, 1980) NGC 5728 (Rubin, 1980), NGC 4490 (Duval, 1981), NGC 1313 (Marcelin and Athanassoula, 1982), NGC 253 and NGC 5236 (de Vaucouleurs *et al.*, 1983), NGC 6221 (Pence and Blackman, 1984).

This reality was at first disputed by Blackman and Pence (1982), when they argued that only pure circular motions were present in NGC 2525 and NGC 7741 (opposite to the result presented here, but which cannot be discussed as they have published data only along the major axis of the bar). They also argued that the previous data on NGC 1300 and NGC 5383 could be explained without gas flows associated with the bars, which for NGC 5383 does not seem supported by the more extensive results of Duval and Athanassoula (1983).

Evidence in favour of the « S » distortion has been presented by Peterson (1984) for one of the galaxies studied here (NGC 7479) as well as for NGC 1097, NGC 1566, and NGC 7496. As we have seen, clear « S » distortions are found in this paper for the three objects studied. The same effect (Duval and Monnet, in preparation) has been also found for the Large Magellanic Cloud.

Very few M/L ratios have been obtained so far for the bar component : the results presented here more than doubled the previous determinations (NGC 5383, Duval and Athanassoula, 1983; NGC 1313, Marcelin and Athanassoula, 1982). They confirm rather normal values, i.e. quite close to that of the surrounding disk. This supports the simple picture of the bars, as a density wave in the disk, without strong preference for either young or old stellar populations. It must be pointed out, however, that the present study is quite preliminary : a much better spatial coverage would be needed to take into account the (probable) shocks across the dust lanes in the bar. The accuracy of the M/L ratios for the bars is rather poor (at least a factor 1.5 uncertainty), mainly for the same reason. The new technique of two-dimensional scanning Fabry-Perot interferometry can generate such data with a very good efficiency, and we have already in progress a study on NGC 3351. Of course a more sophisticated theoretical analysis will be needed.

Appendix. — DETERMINATION OF THE AXISYMMETRIC « ROTATION » CURVE AND OF THE MASS OF THE BAR IN A BARRED SPIRAL. — With the pure rotation $U_{\theta,0}(\rho)$ only, the radial velocity at a point ρ, θ (polar coordinates in the plane of the galaxy) is $V_p = U_{\theta,0}(\rho) \cos\theta \sin i$ (i = inclination). For a linear perturbation of the gravitational potential, due to the bar, we adopt

$$\phi(\rho) = \phi_o(\rho) + \sum_{m=2,4\ldots} \phi_m(\rho) \exp[im(\Omega_p\, t - \theta)]\,.$$

The linearized Euler equations, for negligible viscosity of the gas flow (Ω_p real) and the absence of shocks, give for the corresponding perturbations of the rotation velocity $U_{\theta,0}(\rho)$ and the expansion velocity $U_{\rho,m}(\rho)$ (Athanassoula, 1978) :

$$U_{\theta,m} = \frac{\rho^{-3/2}}{\kappa^2(1-\nu^2)}\left[-m\nu\kappa + \frac{\kappa^2}{2\,\Omega}\left(\rho\frac{\partial}{\partial\rho} - \frac{1}{2}\right)\right] \times (\rho^{1/2}\,\phi_m) \quad (1)$$

$$U_{\rho,m} = \frac{im\,\rho^{-3/2}}{\kappa^2(1-\nu^2)}\left[2\,\Omega - \frac{\nu\kappa}{m}\left(\rho\frac{\partial}{\partial\rho} - \frac{1}{2}\right)\right](\rho^{1/2}\,\phi_m) \quad (2)$$

where κ is the epicyclic frequency :

$$\kappa = 2\,\Omega\left[1 + \frac{\Omega}{2\,\rho}\frac{d\Omega}{d\rho}\right]^{1/2}$$

Ω the angular velocity :

$$\Omega = U_{\theta,0}/\rho$$

ν the frequency of a particle passing through the bar :

$$\nu = m(\Omega_p - \Omega)/\kappa\,.$$

For a bar which sets at an angle θ_o with the line of nodes, the predicted radial velocity at point (ρ, θ) is :

$$V_p(\rho,\theta) = U_{\theta,0}(\rho)\cos\theta \sin i + \sum_{m=2,4\ldots} U_{\rho,m}^{\theta,m}(\rho) \,{}^{\cos}_{\sin}\, m(\theta-\theta_o)\,{}^{\cos}_{\sin}\,\theta \sin i\,. \quad (3)$$

1. *Determination of the axisymmetric « rotation » curve : $U_{\theta,0}(\rho)$.*

Equation (3) multiplied by $\frac{\sin(2\,\theta_o - \theta)}{\sin i}\,d\theta$ and integrated over θ from $-\frac{\pi}{2}$ to $+\frac{\pi}{2}$ gives :

$$\frac{1}{\sin i}\int_{-\frac{\pi}{2}}^{+\frac{\pi}{2}} V_p(\rho)\sin(2\,\theta_o - \theta)\,d\theta =$$

$$= \frac{\pi}{2}\sin 2\,\theta_o\,U_{\theta,0}(\rho) \sum_{m=2,4\ldots} A_m\,\theta_{\theta,m}(\rho) + \sum_{m=2,4\ldots} B_m\,U_{\rho,m}(\rho)$$

with

$$A_m \equiv \int_{-\frac{\pi}{2}}^{+\frac{\pi}{2}} \cos m(\theta - \theta_o)\cos\theta\sin(2\,\theta_o - \theta)\,d\theta \equiv 0$$

for all m even. And

$$B_m \equiv \int_{-\frac{\pi}{2}}^{+\frac{\pi}{2}} \sin m(\theta - \theta_o)\sin\theta\sin(2\,\theta_o - \theta)\,d\theta \equiv 0$$

for all m.

The rotation curve $U_{\theta,0}(\rho)$ is thus obtained by :

$$U_{\theta,0}(\rho) = \frac{2}{\pi \sin i \sin 2\,\theta_o}\int_{-\frac{\pi}{2}}^{+\frac{\pi}{2}} V_p(\rho)\sin(2\,\theta_o - \theta)\,d\theta \tag{4}$$

except if $\theta_o \simeq 0$ or $\frac{\pi}{2}$, in which cases the influence of the bar cannot be separated from a pure rotation law.

A cruder method uses $V_p/\sin i$ along the lines of nodes ($\theta = 0°$) as close to $U_{\theta,0}$, which is quite valid as shown below.

Equation (3) gives

$$V_p/\sin i = U_{\theta,0}(\rho) + \sum_{m=2,4\ldots} U_{\theta,0}(\rho)\cos m\theta_o$$

and we need

$$\frac{\Delta U_{\theta,0}}{U_{\theta,0}} = \frac{1}{U_{\theta,0}}\sum U_{\theta,m}\cos m\theta_0 \ll 1\,.$$

Full computation from equation (2) and for the three galaxies studied in the paper shows that the maximum error occurs close to the end of the bar. At this point we have :

$$\nu = 0 \text{ (see Sect. 3.4)}\,,$$

$$\kappa \simeq 2\,\Omega \text{ (from rotation curve in Sect. 3.3)}\,.$$

Equation (2) gives then :

$$\frac{\Delta U}{U} = \frac{\lambda_B}{U_{\theta,0}^2}\left[\alpha\frac{d\phi_2}{d\alpha}\cos 2\theta_o + \alpha\frac{d\phi_4}{d\alpha}\cos 4\,\theta_o\right]$$

where α is the normalized radius $\alpha = \rho/a_B$ (= 1 at the end of the bar) λ is a normalizing coefficient to get $\alpha\frac{d\phi}{d\alpha}$ in $km^2\ s^{-2}$ where $\frac{d\phi}{d\alpha}$ is expressed in « a dimensional » Monnet-Simien (1977) units.

$\lambda_B = 0.0172\ f_B\ I'_{oB}\ q_{aB}\ a_B$
f_B : mass to light ratio of the bar in solar units (Sect. 3.4)
I'_{oB} : observed central luminosity in $L_\odot\ pc^{-2}$
q_{aB} : observed axial ratio (Table II)
a_B : semi-major axis of the bar in pc.

For a mean true axial ratio $q = 0.25$, the Fourier components of an homogeneous bar ($n = 0$), at the end of the bar are :

$$\frac{d\phi_2}{d\alpha} = 0.692\,,\quad \frac{d\phi_4}{d\alpha} = 0.388$$

and the terms of higher order are negligible,

for NGC 3359 : $\lambda_B = 3773\ km^2\ s^{-2}$, $U_{\theta,0} = 103\ km\ s^{-1}$, $\theta_o = 29°$

$$\frac{\Delta U}{U} = 0.07$$

for NGC 7479 : $\lambda_B = 6974\ km^2\ s^{-2}$, $U_{\theta,0} = 212\ km\ s^{-1}$, $\theta_o = 10°$

$$\frac{\Delta U}{U} = 0.15$$

which are indeed $\ll 1$ and the approximation is quite justified.

2. *Determination of the mass of the bar.*

With again $\nu = 0$, at the end of the bar, equation (3) gives :

$$V_p = U_{\theta,0}\cos\theta_o\sin i\left(1 + \frac{\lambda_B}{2\,U_{\theta,0}^2}\sum_{m=2,4\ldots}\alpha\frac{d\phi_m}{d\alpha}\right) \tag{5}$$

where V_p and $U_{\theta,0}$ are in km s^{-1}.

From the known values of $U_{\theta,0}$ and V_p at the end of the bar, equation (5) gives λ_B, and hence the M/L ratio of the bar by :

$$\lambda_B = 2\,U_{\theta,0}^2(V_p/U_{\theta,0}\cos\theta_o\sin i - 1)\Big/\sum_{m=2,4}\alpha\frac{d\phi_m}{d\alpha}$$

for NGC 7741 $\quad q = 0.23 \quad \sum_{m=2,4}\alpha\frac{d\phi}{d\alpha} = 1.107$

for NGC 3359 $\quad q = 0.28 \quad \sum_{m=2,4}\alpha\frac{d\phi}{d\alpha} = 1.062$

for NGC 7479 $\quad q = 0.25 \quad \sum_{m=2,4}\alpha\frac{d\phi}{d\alpha} = 1.080\,.$

References

ATHANASSOULA, E. : 1978, *Astron. Astrophys.* **69,** 395.
BENEDICT, G. : 1982, *Astron. J.* **87,** 86.
BIGAY, J., DUMONT, F., LENOUVEL, F., LUNEL, M. : 1953, *Ann. Astrophys.* **16,** 133.
BLACKMAN, C., PENCE, W. : 1982, *Monthly Notices Roy. Astron. Soc.* **198,** 517.
BLACKMAN, C. : 1983, *Monthly Notices Roy. Astron. Soc.* **202,** 379.
BOTTINELLI, L., GOUGUENHEIM, L., PATUREL, G., DE VAUCOULEURS, G. : 1980, *Astrophys. J.* **242,** L153.
BOTTINELLI, L., GOUGUENHEIM, L., PATUREL, G., DE VAUCOULEURS, G. : 1984, *Astron. Astrophys. Suppl. Ser.* **56,** 381.
DUVAL, M. F. : 1981, *Astron. Astrophys.* **98,** 352.
DUVAL, M. F., ATHANASSOULA, E. : 1983, *Astron. Astrophys.* **121,** 297.
HOLMBERG, E. : 1958, *Medd. Lunds Astron. Obs.* **2,** No. 136.
KALNAJS, A. : 1978, *IAU Symp.* No. **77** (Reidel) p. 123.
KUZ'MIN, G. : 1953, *Tartu Astron. Obs.* **32,** 5, 332.
LONGO, G., DE VAUCOULEURS, A. : 1983, *A general Catalogue of Photoelectric Magnitudes and colors in the U, B, V System.*
MARCELIN, M., ATHANASSOULA, E. : 1982, *Astron. Astrophys.* **105,** 76.
MONNET, G., SIMIEN, F. : 1977, *Astron. Astrophys.* **56,** 173.
OKAMURA, S. : 1978, *Publ. Astron. Soc. Japan* **30,** 91.
PENCE, W. D., BLACKMAN, C. P. : 1984, *Monthly Notices Roy. Astron. Soc.* **207,** 9.
PETERSON, C. : 1984, *Bull. Am. Astron. Soc.* **16,** 540.
PETERSON, C., HUNTLEY, J. : 1980, *Astrophys. J.* **242,** 913.
PETERSON, C., RUBIN, V., FORD, W., THONNARD, N. : 1978, *Astrophys. J.* **219,** 31.
PETTIT, E. : 1954, *Astrophys. J.* **120,** 413.
RUBIN, V. : 1980, *Astrophys. J.* **238,** 808.
SANDAGE, A., TAMMANN, G. A. : 1981, *A revised Shapley-Ames Catalogues.*
STEBBINS, J., WITFORD, A. : 1937, *Astrophys. J.* **86,** 247.
TIFFT, W. : 1963, *Astron. J.* **68,** 302.
TOOMRE, A. : 1963, *Astrophys. J.* **138,** 385.
DE VAUCOULEURS, G. : 1962, *IAU Symp.* No. **15,** 3.
DE VAUCOULEURS, G., DE VAUCOULEURS, A. : 1972, *Mem. Roy. Astron. Soc.* **77,** Part 1.
DE VAUCOULEURS, G., FREEMAN, K. : 1972, *Vistas Astron.* **14,** 163.
DE VAUCOULEURS, G., PENCE, W., DAVOUST, E. : 1983, *Astrophys. J. Suppl. Ser.* **53,** 17.
DE VAUCOULEURS, G., DE VAUCOULEURS, A., CORWIN, H. G. : 1976, *Second Reference Catalogue of Bright Galaxies* (Austin, Univ. Texas Press) (RC2).

TABLE Ia. — *Mean luminosity distribution in NGC 7741.*

log I	μ_B	$\mathcal{A}$	r*	L(r*)	k(r*)	log ρ*	m(ρ*)
0.8	20.00	0.000	0.000	0.000	0.000	-	-
0.7	20.25	0.002_6	0.028_5	0.014_4	0.004_4	-1.45	17.72
0.6	20.50	0.015	0.069	0.072	0.022	-1.07	15.97
0.5	20.75	0.034	0.104	0.141	0.043	-0.89	15.25
0.4	21.00	0.059	0.137	0.211	0.065	-0.77	14.81
0.3	21.25	0.080	0.160	0.260	0.080	-0.70	14.58
0.2	21.50	0.120	0.195	0.330	0.102	-0.62	14.32
0.1	21.75	0.186	0.243	0.425	0.131	-0.52	14.05
0.0	22.00	0.313	0.316	0.568	0.175	-0.41	13.73
-0.1	22.25	0.518	0.406	0.752	0.231	-0.30	13.43
-0.2	22.50	0.870	0.526	1.002	0.308	-0.19	13.12
-0.3	22.75	1.474	0.685	1.344	0.413	-0.07	12.80
-0.4	23.00	2.279	0.852	1.707	0.525	0.02	12.54
-0.5	23.25	3.100	0.993	2.000	0.615	0.08	12.37
-0.6	23.50	4.059	1.137	2.271	0.698	0.15	12.23
-0.7	23.75	4.952	1.255	2.472	0.760	0.19	12.14
-0.8	24.00	5.995	1.381	2.659	0.818	0.23	12.06
-0.9	24.25	6.706	1.461	2.760	0.849	0.26	12.02
-1.0	24.50	7.333	1.528	2.831	0.871	0.28	11.99
-1.1	24.75	8.019	1.598	2.893	0.890	0.29	11.97
-1.2	25.00	8.661	1.660	2.938	0.904	0.31	11.95
-1.3	25.25	9.091	1.701	2.963	0.911	0.32	11.94
-1.4	25.50	9.543	1.743	2.983	0.918	0.33	11.93
-1.5	25.75	10.436	1.823	3.015	0.927	0.35	11.92
-1.6	26.00	11.304	1.897	3.040	0.935	0.37	11.91
-1.7	26.25	12.034	1.957	3.056	0.940	0.38	11.90
-1.8	26.50	14.586	2.155	3.102	0.954	0.42	11.89
-1.9	26.75	16.774	2.311	3.133	0.964	0.46	11.88
-2.0	27.00	18.962	2.457	3.158	0.971	0.48	11.87
∞	-	-	-	3.251	1.000	-	11.84

TABLE Ib. — *Mean luminosity distribution in NGC 3359.*

log I	μ_B	$\mathcal{A}$	r*	L(r*)	k(r*)	log ρ*	m(ρ*)
0.8	19.60	0.000	0.000	0.000	0.000	-	-
0.7	19.85	0.001_8	0.024_1	0.010_3	0.002_2	-1.64	17.68
0.6	20.10	0.005_8	0.043_1	0.028_4	0.006_1	-1.39	16.58
0.5	20.35	0.013_9	0.066_4	0.057_0	0.012_2	-1.20	15.82
0.4	20.65	0.030	0.098	0.104	0.023	-1.03	15.14
0.3	20.85	0.054	0.132	0.158	0.034	-0.90	14.71
0.2	21.10	0.095	0.174	0.232	0.050	-0.78	14.29
0.1	21.35	0.174	0.235	0.344	0.073	-0.65	13.88
0.0	21.60	0.392	0.353	0.590	0.126	-0.48	13.29
-0.1	21.85	0.835	0.516	0.987	0.211	-0.31	12.73
-0.2	22.10	1.315	0.647	1.328	0.284	-0.21	12.41
-0.3	22.35	1.991	0.796	1.711	0.365	-0.12	12.13
-0.4	22.60	2.943	0.968	2.140	0.457	-0.04	11.89
-0.5	22.85	3.723	1.089	2.418	0.516	0.01	11.76
-0.6	23.10	4.522	1.200	2.644	0.564	0.06	11.66
-0.7	23.35	5.455	1.318	2.854	0.609	0.10	11.58
-0.8	23.60	7.034	1.496	3.137	0.670	0.15	11.47
-0.9	23.85	8.697	1.664	3.375	0.721	0.20	11.40
-1.0	24.10	10.652	1.841	3.596	0.768	0.24	11.33
-1.1	24.35	13.565	2.078	3.857	0.823	0.29	11.25
-1.2	24.60	15.647	2.232	4.005	0.855	0.33	11.21
-1.3	24.85	17.868	2.385	4.131	0.882	0.35	11.18
-1.4	25.10	20.785	2.572	4.262	0.910	0.39	11.14
-1.5	25.35	22.806	2.694	4.334	0.925	0.41	11.12
-1.6	25.60	23.980	2.763	4.367	0.932	0.42	11.11
-1.7	25.85	26.255	2.891	4.419	0.943	0.44	11.10
-1.8	26.10	29.472	3.063	4.476	0.956	0.46	11.09
∞	-	-	-	4.684	1.000	-	11.04

TABLE Ic. — *Mean luminosity distribution in NGC 7479.*

log I	μ_B	$\mathcal{A}$	r*	L(r*)	k(r*)	log ρ*	m(ρ*)
0.7	19.78	0.000	0.000	0.000	0.000	-	-
0.6	20.03	0.002_9	0.030_5	0.013_1	0.004_6	-1.48	17.34
0.5	20.28	0.008_4	0.051_7	0.032_6	0.011_6	-1.25	16.35
0.4	20.53	0.018_6	0.076_9	0.061_6	0.021_8	-1.08	15.66
0.3	20.78	0.035	0.106	0.099	0.035	-0.94	15.14
0.2	21.03	0.063	0.141	0.148	0.053	-0.81	14.71
0.1	21.28	0.132	0.205	0.244	0.088	-0.65	14.15
0.0	21.53	0.238	0.275	0.366	0.130	-0.52	13.72
-0.1	21.78	0.409	0.361	0.520	0.185	-0.41	13.34
-0.2	22.03	0.618	0.443	0.669	0.238	-0.32	13.07
-0.3	22.28	0.875	0.528	0.814	0.289	-0.24	12.86
-0.4	22.53	1.211	0.621	0.966	0.343	-0.17	12.67
-0.5	22.78	1.661	0.727	1.126	0.400	-0.10	12.50
-0.6	23.03	2.476	0.888	1.357	0.482	-0.02	12.30
-0.7	23.28	3.476	1.052	1.582	0.562	0.06	12.14
-0.8	23.53	4.719	1.226	1.804	0.641	0.12	11.99
-0.9	23.78	5.743	1.352	1.951	0.693	0.17	11.91
-1.0	24.03	6.494	1.438	2.026	0.724	0.19	11.86
-1.1	24.28	7.756	1.571	2.149	0.764	0.23	11.80
-1.2	24.53	8.679	1.662	2.214	0.787	0.26	11.77
-1.3	24.78	9.289	1.719	2.249	0.799	0.27	11.75
-1.4	25.03	11.618	1.923	2.354	0.836	0.31	11.70
-1.5	25.28	14.065	2.116	2.441	0.867	0.36	11.66
-1.6	25.53	16.620	2.300	2.513	0.893	0.40	11.63
-1.7	25.78	19.772	2.509	2.584	0.918	0.43	11.60
∞	-	-	-	2.814	1.000	-	11.51

TABLE II. — *Luminosity parameters.*

			NGC 7741	NGC 3359	NGC 7479
Total Apparent magnitude	B_T		11.84 ± 0.04	11.04 ± 0.05	11.51 ± 0.06
Corrected apparent magnitude	B_T^o		11.41	10.61	11.12
Distance moduli	μ^o		30.11	30.53	31.79
Corrected absolute magnitude	M_T^o		-18.70	-19.92	-20.67
Corrected total luminosity	$L_T^o/L_\odot$		4.4 10^9	1.4 10^{10}	2.7 10^{10}
Components - B band (sky plane)					
Bar	p.a.	°	98	12	8
	q_a		0.30	0.30	0.25
	a'_o	'arc	0.55	0.58	0.92
	I'_o	mag(")$^{-2}$	20.42*	20.09*	22.24
Central disk	p.a.	°	170 to 160	160	35
	q_a		0.81 to 0.71	0.78	0.77
	I'_o	mag(")$^{-2}$	22.87	22.25	23.45
Extended disk	p.a.	°	160	175	15
	q_a		0.71	0.56	0.72
	I'_o	mag(")$^{-2}$	23.25	22.35	22.83
Inclination	i	°	45 ± 2	57 ± 3	45 ± 2
Luminosity model - B band (galaxy plane)					
Bar	n		6	8	0
	q		0.23	0.28	0.25
	a_o	'arc	0.73	0.64	0.93
	θ_o	°	69	29	10
Central disk	n		2	1	2
	a_o	'arc	2.12	1.50	1.93
Extended disk	a_e	'arc	1.42	1.95	1.75

* These values are affected by star formation

TABLE III. — *Relative* (L/L_T) *contributions.*

	Bulge	Bar	Central disk	Extended disk	Arms
NGC 7741	-	0.09	0.56	0.31	0.04
NGC 3359	-	0.05	0.31	0.49	0.15
NGC 7479	0.13	0.08	0.24	0.53	0.02

TABLE V.

			NGC 7741	NGC 3359	NGC 7479
Kuz'min-Toomre disks					
n° 1	A_1	$km^2 s^{-2}$ 'arc	47 397	164 531	340 312
	a_1	'arc	2,02	2,02	1,73
n° 2	A_2	$km^2 s^{-2}$ 'arc	3178	4597	10 235
	a_2	'arc	0,62	0,49	0,62
Radius of the bar	a_B	'arc	0,73	0,64	0,93
Integrated mass	$M(a_B)$	$M_\odot$	2,81 10^9	8,19 10^9	6,97 10^{10}
Integrated luminosity	$L(a_B)$	$L_\odot$	1,11 10^9	2,03 10^9	7,84 10^9
Total luminosity of the bar	$L_{T,B}$	$L_\odot$	4,34 10^8	5,53 10^8	1,51 10^9
Apparent M/L (a_B)		$M_\odot/L_\odot$	2,53	4,03	8,89

TABLE VI.

		NGC 7741	NGC 3359	NGC 7479
V_p	km s^{-1}	25	90	160
$U_{\theta,o}(a_B)$	km s^{-1}	66	103	212
λ_B	$km^2 s^{-2}$	3852	3773	6974
Apparent $(M/L)_B$	$M_\odot/L_\odot$	0,80	0,54	3,36
Corrected $(M/L)_B$	$M_\odot/L_\odot$	0,54	0,36	2,53
Apparent $(M/L)^*_B$	$M_\odot/L_\odot$	4,96	5,45	-
Corrected $(M/L)^*_B$	$M_\odot/L_\odot$	3,34	3,67	-
Apparent $(M/L)_a$	$M_\odot/L_\odot$	3,64	5,33	10,20
Corrected $(M/L)_a$	$M_\odot/L_\odot$	2,45	3,59	7,67

TABLE IVa. — *Radial velocities in NGC 7741.*

X	Y	V(Hα)	V(NII)
I1551			
(// to the bar)			
-58.3	-5.1	695	
-55.7	-4.9	702	
-53.1	-4.6	715	
-50.5	-4.4	720	
-47.9	-4.2	726	
-45.3	-4.0	730	
-42.7	-3.7	730	
-40.1	-3.5	735	
-37.5	-3.3	728	
-35.0	-3.1	730	
-32.4	-2.8	731	
-29.8	-2.6	728	
-27.2	-2.4	755	
-24.6	-2.2	745	
-22.0	-1.9	759	
-19.4	-1.7	760	
-16.8	-1.5	760	
-14.2	-1.2	756	
-11.6	-1.0	757	
-9.1	-0.8	756	
-6.5	-0.6	755	
-3.9	-0.4	755	
-1.3	-0.1	760	765
1.3	0.1	754	748
3.9	0.4	749	751
6.5	0.6	745	756
9.1	0.8	752	756
11.6	1.0	760	758
14.2	1.2	756	
16.8	1.5	755	
19.4	1.7	750	
22.0	1.9	746	
24.6	2.2	767	
27.2	2.4	777	
29.8	2.6	779	
32.4	2.8	769	
35.0	3.1	765	
37.5	3.3	761	
40.1	3.5	767	
42.7	3.7	781	

X	Y	V(Hα)
45.3	4.0	801
47.9	4.2	796
50.5	4.4	796
53.1	4.6	796
55.7	4.9	805
I1562		
(// to the bar)		
-51.8	-4.5	697
-49.2	-4.3	706
-46.6	-4.1	735
-44.0	-3.9	737
-41.4	-3.6	739
-38.8	-3.4	735
-36.3	-3.2	732
-33.7	-2.9	736
-28.5	-2.5	739
-25.9	-2.3	743
-23.3	-2.0	737
-20.7	-1.8	753
-18.1	-1.6	749
-15.5	-1.4	751
-13.0	-1.1	746
-10.4	-0.9	745
-7.8	-0.7	750
-5.2	-0.5	752
-2.6	-0.3	757
0.0	0.0	750
2.6	0.3	747
5.2	0.5	755
7.8	0.7	750
10.4	0.9	744
13.0	1.1	750
15.5	1.4	753
18.1	1.6	755
20.7	1.8	764
23.3	2.0	758
25.9	2.3	777

X	Y	V(Hα)
28.5	2.5	781
31.1	2.7	764
33.7	2.9	754
36.3	3.2	762
38.8	3.4	765
41.4	3.6	764
I1563		
(// to the bar)		
-17.5	-20.1	728
-13.1	-19.7	729
-8.8	-19.4	726
-4.4	-19.0	728
0.0	-18.7	730
4.4	-18.3	733
8.8	-18.0	735
13.2	-17.3	735
I1663		
(// to the bar)		
-66.4	-1.8	697
-63.8	-1.6	697
-61.2	-1.4	704
-58.6	-1.2	719
-56.0	-0.9	725
-54.4	-0.7	714
-50.8	-0.5	714
-48.5	-0.2	722
-45.7	0.0	719
-43.1	0.2	718
-40.5	0.5	720
-37.9	0.7	736
-35.3	0.9	745
-32.7	1.1	752
-30.1	1.4	766
-27.5	1.6	763
-24.9	1.8	766
-22.3	2.0	766
-19.7	2.3	760
-17.1	2.5	759

X	Y	V(Hα)	V(NII)
-14.6	2.7	773	
-12.0	3.0	775	
-9.4	3.2	779	789
-6.8	3.4	783	790
-4.2	3.6	785	786
-1.6	3.9	784	778
1.0	4.1	774	769
3.6	4.3	765	765
6.2	4.5	761	774
8.8	4.8	769	
11.4	5.0	762	
14.0	5.2	764	
16.6	5.4	774	
19.1	5.7	771	
21.7	5.9	770	
24.3	6.1	765	
26.9	6.4	766	
29.5	6.6	778	
32.1	6.8	766	
34.7	7.0	771	
37.3	7.3	769	
39.9	7.5	761	
I1668			
(// to the bar)			
-62.2	-9.5	685	
-59.6	-9.2	698	
-57.0	-9.0	700	
-54.4	-8.8	699	
-51.8	-8.5	703	
-49.2	-8.3	722	
-46.6	-8.1	710	
-44.0	-7.9	703	
-41.4	-7.6	705	
-38.8	-7.4	713	
-36.3	-7.2	725	
-33.5	-6.9	722	
-30.9	-6.7	724	
-28.5	-6.5	742	
-25.9	-6.3	741	

TABLE IVa (*continued*).

X	Y	V(Hα)
-23.3	-6.1	743
-20.7	-5.8	735
-18.1	-5.6	746
-15.5	-5.4	745
-13.0	-5.1	741
-10.4	-4.9	746
-7.8	-4.7	746
-5.2	-4.5	751
-2.6	-4.2	754
0.0	-4.0	742
2.6	-3.8	743
5.2	-3.5	749
7.8	-3.3	753
10.4	-3.1	743
13.0	-2.9	728
18.1	-2.4	756
20.7	-2.2	740
23.3	-2.0	739
25.9	-1.7	769
28.5	-1.5	776
30.9	-1.3	744
36.3	-0.8	745
12103		
-12.6	-71.7	681
-12.2	-59.1	685
-11.7	-66.6	682
-11.3	-64.0	685
-10.8	-61.5	686
-10.4	-58.9	694
-9.5	-53.8	698
-9.0	-51.2	699
-8.6	-48.6	709
-8.1	-46.1	737
-7.7	-43.5	731
-7.2	-41.0	734
-6.8	-38.4	751
-5.9	-33.3	696
-5.4	-30.7	705

X	Y	V(Hα)	V(NII)
-5.0	-28.2	711	
-3.6	-20.5	719	
-3.2	-17.9	721	
-1.8	-10.2	725	
-1.4	-7.7	730	719
-0.9	-5.1	750	748
-0.5	-2.6	754	753
0.0	0.0	755	757
0.5	2.6	760	763
0.9	5.1	761	765
1.4	7.7	770	760
1.8	10.2	771	
2.3	12.8	775	
2.7	15.4	768	
3.2	17.9	791	
10.8	61.5	803	
11.3	54.0	813	
11.7	66.6	822	
12.2	59.1	814	
12.6	71.7	827	
13.1	74.2	824	
13.5	76.8	813	
14.0	79.4	818	
14.4	81.9	819	
14.9	84.5	823	
15.4	87.0	829	
15.8	89.6	824	
16.3	92.2	817	
16.7	94.7	821	
17.2	97.3	812	
17.6	99.9	820	
BTA23			
-129.3	-41.3	709	
-100.5	-40.0	711	
-84.3	-12.0	704	
-75.5	-52.5	719	
-75.5	-19.8	693	

X	Y	V(Hα)
-37.0	-9.5	705
-31.5	-8.3	715
-23.5	41.0	761
-20.0	-7.0	753
-18.5	-7.5	740
-17.0	-25.5	727
-16.0	20.0	753
-15.8	-130.3	675
-15.5	5.5	785
-15.0	-6.3	732
-11.0	20.0	766
-10.0	-128.3	681
-6.8	4.8	794
-5.8	-26.8	730
-6.0	20.0	757
0.0	-100.0	673
2.0	-26.0	732
2.3	19.0	772
2.5	-8.3	753
4.5	-27.8	733
8.8	6.3	753
11.5	-8.8	724
11.8	4.5	753
13.8	-19.5	734
14.3	-9.8	730
17.3	-33.0	726
19.8	4.0	744
23.3	12.5	790
29.0	-18.5	735
30.8	-45.8	722
31.5	-3.5	752
32.0	-47.0	721
32.5	-111.3	664
37.5	5.8	789
38.0	-90.3	727
41.3	-4.5	778
50.3	-58.5	717
54.8	-96.5	740
56.5	-24.8	745
58.0	-28.0	743

X	Y	V(Hα)
58.0	29.0	813
60.0	-30.5	748
66.2	-64.6	748
67.5	-17.5	735
68.8	-148.8	731
76.5	55.8	830
79.0	-64.3	744
80.0	-58.5	724
80.0	-18.3	760
87.5	-123.8	726
90.5	0.0	786
90.5	-67.0	766
91.5	-110.0	745
101.0	-56.3	777
101.3	-111.8	759
111.0	-68.8	773
BTA24		
-81.8	5.0	700
-67.0	43.8	750
-60.5	54.8	758
-52.0	70.0	776
-44.3	-18.3	688
-42.5	-9.3	715
-41.0	0.8	746
-41.0	89.0	805
-39.3	9.8	754
-38.0	90.3	805
-35.5	-1.0	731
-35.5	32.3	770
-33.0	46.0	785
-31.3	31.5	770
-29.0	-35.3	693
-28.5	-28.0	701
-28.0	-19.5	727
-27.8	52.3	797
-27.5	-11.3	746
-26.5	8.0	758

X	Y	V(Hα)
-26.5	85.0	803
-26.0	17.5	758
-25.0	30.5	777
-25.0	84.8	805
-21.3	-19.0	735
-21.0	-10.8	741
-19.5	84.3	810
-15.5	7.8	757
-10.0	81.3	820
-12.3	44.5	787
-8.8	87.3	820
-6.0	-1.8	755
-5.0	5.0	791
-2.3	-19.5	734
-1.3	-26.3	728
-0.3	1.0	780
0.0	46.8	795
0.0	88.0	822
1.5	-9.0	736
7.5	108.0	828
8.0	4.0	776
21.0	-36.8	726
22.5	-21.3	729
22.5	118.0	819
27.5	30.5	800
29.3	44.8	797
37.0	11.3	792
38.3	34.5	817
58.3	-3.3	794
63.8	80.8	822
74.0	108.8	828

TABLE IVb. — *Radial velocities in NGC 3359.*

X	Y	V(Hα)	V(NII)
I1316 (// to the bar)			
6.6	-46.8	919	
6.2	-44.3	918	919
5.8	-41.7	914	909
5.5	-39.1	923	923
5.1	-36.5	935	939
4.8	-34.0	937	
4.4	-31.4	912	
4.0	-28.8	926	
3.7	-26.2	945	964
3.3	-23.7	945	960
3.0	-21.1	955	959
2.6	-18.5	945	954
2.3	-15.9	960	973
1.9	-13.4	976	979
1.5	-10.8	984	992
1.2	-8.2	987	987
0.8	-5.6	986	985
0.4	-3.1	988	989
0.1	-0.5	1006	1001
-0.3	2.1	996	996
-0.6	4.7	995	986
-1.0	7.2	1003	993
-1.4	9.8	1006	1007
-1.7	12.4	1009	1021
-2.1	15.0	1023	1032
-2.5	17.5	1026	
-2.8	20.1	1039	1037
-3.2	22.7		1037
-3.5	25.4	1049	1027
-3.9	28.0	1043	1025
-4.3	30.5	1074	1092
-4.6	33.2	1078	1086
-5.0	35.8	1075	1072
-5.4	38.3	1085	1082
-5.7	41.0	1091	1096
-6.1	43.6	1099	1102
-6.4	46.2	1092	
-6.8	47.7	1120	

X	Y	V(Hα)	V(NII)
I1324			
2.4	-45.4	911	
2.3	-42.8	912	
2.1	-40.2	914	
2.0	-37.6	925	
1.8	-35.0	920	
1.6	-29.3	934	
1.4	-27.3	947	
1.3	-24.7	973	
1.2	-22.1	980	
1.0	-19.5	962	
0.9	-16.9	973	
0.7	-14.3	980	
0.6	-11.7	993	993
0.5	-9.1	999	1005
0.4	-6.5	995	
0.2	-3.9	998	
0.1	-1.3	998	
-0.1	1.3	999	
-0.2	3.9	1005	
-0.4	6.5	1010	
-0.5	9.1	1011	
-0.9	16.9	1040	
-1.0	19.5	1046	
-1.2	22.1	1040	
-1.3	24.7	1032	
-1.4	27.3	1031	
-1.6	29.8	1037	
-1.7	32.5	1120	
-1.8	35.0	1124	
-2.0	37.5	1123	
-2.1	40.2	1110	
-2.3	42.8	1103	
-2.4	45.4	1076	
-2.5	48.0	1090	
-2.6	50.5	1093	
-2.8	53.2	1110	
-2.9	55.8	1127	
-3.1	58.4	1140	
-3.2	61.0	1138	
-3.3	53.5	1110	

X	Y	V(Hα)	V(NII)
-3.5	66.2	1122	
-3.6	68.8	1134	
-3.7	71.4	1125	
-3.9	74.0	1124	
I1584			
-43.4	8.4	1063	
-40.8	7.9	1060	
-38.3	7.4	1048	
-35.7	6.9	1042	
-33.2	6.4	1050	
-30.6	6.0	1065	
-28.1	5.5	1057	
-25.5	5.0	1057	
-23.0	4.5	1066	
-20.4	4.0	1038	
-17.9	3.5	1042	
-15.3	3.0	1034	
-12.8	2.5	1034	
-10.2	2.0	1013	
-7.7	1.5	998	
-5.1	1.0	996	
-2.5	0.5	995	
0.0	0.0	1002	
2.5	-0.5	1007	
5.1	-1.0	1011	
7.7	-1.5	996	
10.2	-2.0	990	
12.8	-2.5	993	
15.3	-3.0	995	
17.9	-3.5	1004	
20.4	-4.0	995	
28.1	-5.5	998	
30.6	-6.0	994	
33.2	-6.4	1009	
35.7	-6.9	1008	
38.3	-7.4	990	
40.8	-7.9	997	
43.4	-8.4	1005	

X	Y	V(Hα)	V(NII)
I1585			
-1.1	-39.0	919	
-0.7	-36.4	920	
-0.3	-33.8	932	
0.2	-31.2	922	
0.6	-28.6	941	
1.0	-26.0	948	
2.8	-16.1	970	
3.2	-13.5	981	
3.6	-10.9	969	981
4.1	-8.3	972	975
4.5	-5.7	983	994
4.9	-3.1	982	
5.4	-0.5	983	993
5.8	2.1	972	983
6.2	4.7	978	
6.7	7.3	978	
7.1	9.9	978	
7.6	12.1	1010	
8.5	17.2	1004	
9.4	22.4	1050	
9.8	25.0	1074	
10.2	27.6	1068	
10.7	30.2	1073	
11.1	32.8	1084	
12.0	38.0	1064	
12.9	43.2	1040	
13.4	45.8	1063	
13.8	47.8	1057	
14.2	50.4	1076	
14.7	53.0	1104	
15.1	55.6	1080	
15.5	58.2	1102	
16.0	60.8	1089	
16.4	52.9	1075	
19.0	78.5	1140	
19.5	81.1	1150	
19.9	83.7	1142	
20.4	86.3	1153	
20.7	88.9	1145	
21.2	91.5	1118	

X	Y	V(Hα)	V(NII)
21.6	94.1	1116	
22.0	96.7	1122	
I1590			
22.8	-44.8	921	
21.6	-42.5	928	
20.5	-40.2	941	
19.3	-37.9	930	
18.1	-35.5	953	
16.9	-33.2	967	
15.8	-30.9	971	
14.6	-28.6	962	
13.4	-26.3	968	
12.2	-24.0	980	
11.0	-21.7	986	
9.8	-19.3	993	
8.7	-17.0	998	
7.5	-14.7	999	
6.3	-12.4	1006	
5.1	-10.1	1011	
3.9	-7.7	1006	
2.8	-5.4	999	
1.6	-3.1	997	
0.4	-0.4	1005	
-0.8	1.5	990	
-1.9	3.3	1000	
-3.1	6.1	1003	
-4.3	8.5	1005	
-5.5	10.8	1006	
-6.7	13.1	1020	
-7.8	15.4	1013	
-9.0	17.7	1022	
-10.2	20.0	1036	
-11.4	22.4	1028	
-12.6	24.7	1040	
-13.8	27.0	1040	
-14.9	29.3	1059	
-16.1	31.6	1053	
-17.3	33.9	1062	
-18,5	36,3	1060	
-19,7	38,6	1062	

TABLE IVc. — *Radial velocities in NGC 7479.*

X	Y	V(Hα)	V(NII)
11550 (// to the bar)			
-10.0	76.2	2212	
-9.8	73.7	2226	
-9.5	71.1	2230	
-9.2	58.5	2208	
-8.9	65.9	2202	
-8.7	63.4	2223	
-8.4	60.8	2200	
-8.1	58.2	2201	
-7.8	55.6	2203	
-7.6	53.0	2204	
-7.3	50.4	2240	
-7.0	47.8	2235	
-6.8	45.2	2236	
-6.5	42.7	2268	
-6.2	40.1	2264	
-5.9	37.5	2271	
-5.7	34.9	2292	
-5.4	32.3	2300	
-5.1	29.7	2296	
-4.9	27.2	2322	
-4.6	24.6	2330	
-4.3	22.0	2345	
-4.0	19.4	2340	
-3.5	14.2	2374	
-3.2	11.6	2375	2355
-2.9	9.1	2369	2352
-2.7	6.5		2353
-1.9	-1.3	2385	2389
-1.6	-3.9	2385	
-1.3	-6.5	2340	
-1.0	-9.1	2355	
-0.8	-11.6	2363	
-0.5	-14.2	2400	2385
-0.3	-16.8	2407	2402
0.0	-19.4	2403	2389
0.3	-22.0	2420	
0.6	-24.6	2433	
0.8	-27.2	2446	
1.1	-29.7	2436	2460
1.4	-32.3	2460	
1.7	-34.9	2472	
1.9	-37.5	2460	
2.2	-40.1	2485	
2.5	-42.7	2491	
2.8	-45.2	2492	
3.0	-47.8	2514	
3.3	-50.6	2521	
3.6	-53.0	2521	
3.8	-55.6	2535	
11557 (// to the bar)			
-1.0	56.9	2234	
-0.7	54.3	2237	
-0.4	51.7	2240	
-0.2	49.1	2245	
0.1	46.5	2240	2239
0.4	43.9	2254	2240
0.6	41.4	2263	2279
0.9	38.8	2277	2269
1.2	36.2	2287	
1.5	33.6	2291	
1.7	31.0	2298	2297
2.0	28.4	2299	
2.3	25.8	2326	
2.5	23.3	2349	
2.8	20.7	2356	
3.1	18.1	2347	
3.4	15.5	2361	
3.6	12.9	2375	
3.9	10.3	2362	
4.7	2.5	2420	
5.0	0.0	2414	
5.8	-7.8	2469	
6.1	-10.3	2503	
6.4	-12.9	2496	
6.6	-15.5	2498	
7.9	-18.1	2505	
7.3	-20.7	2494	
7.5	-23.3	2488	
7.7	-25.8	2483	
7.9	-28.2	2444	
9.1	-38.8	2486	
9.4	-41.4	2488	
9.6	-43.9	2462	
9.9	-46.5	2474	
10.2	-49.1	2476	
10.4	-51.7	2488	
10.7	-54.3	2489	
11.0	-56.9	2489	
11654 (// to the bar)			
-3.4	61.2	2241	
-3.2	58.7	2237	
-2.9	56.1	2250	
-2.6	53.5	2263	
-2.3	50.9	2270	
-2.0	48.3	2270	
-1.8	45.7	2274	
-1.5	43.2	2263	
-1.2	40.6	2253	
-1.0	38.0	2265	
-0.7	35.4	2260	
-0.4	32.8	2284	
-0.2	30.2	2264	
0.1	27.6	2283	
0.4	25.1	2316	
0.7	22.5	2342	
0.9	19.9	2341	
1.2	17.3	2336	
1.5	14.7	2392	
1.7	12.2	2391	
2.0	9.5	2379	
2.3	7.0	2391	
2.5	4.4	2404	
2.8	1.8	2396	
4.2	-11.1	2367	
4.5	-13.7	2366	
4.8	-16.3	2391	
5.0	-18.9	2485	
5.3	-21.5	2465	
5.6	-24.1	2475	
5.8	-26.6	2493	
6.1	-29.2	2455	
6.4	-31.8	2447	
6.6	-34.4	2452	
6.9	-37.0	2482	
7.2	-39.6	2493	
7.4	-42.2	2480	
7.7	-44.8	2522	
8.0	-47.3	2503	
8.2	-49.9	2525	
9.1	-57.7	2519	
9.3	-50.3	2524	
9.6	-62.9	2527	
9.5	-55.4	2532	
11657 (// to the bar)			
-6.7	64.2	2220	
-6.5	61.6	2216	
-6.2	59.0	2221	
-5.9	56.4	2221	2237
-5.7	53.8	2233	
-5.4	51.2	2225	
-5.1	48.6	2217	2225
-4.8	46.0	2230	2233
-4.6	43.4	2256	
-4.3	40.9	2251	
-4.0	38.3	2245	
-3.8	35.7	2294	
-3.5	33.1	2294	
-3.2	30.5	2299	
-2.9	28.0	2294	
-2.7	25.4	2312	
-2.4	22.6	2314	
-2.1	20.2	2339	
-1.8	17.6	2344	
-1.6	15.0	2351	
-1.3	12.5	2349	
-1.0	9.9	2349	
-0.8	7.3	2342	
-0.2	2.1	2390	
0.1	-0.5	2381	

TABLE IVc (continued).

X	Y	V(Hα)	V(NII)
I 1657			
0.3	-3.1	2385	
0.6	-5.6	2382	
0.9	-8.2	2381	
1.1	-10.8	2372	
1.4	-13.4	2361	
1.7	-15.9	2381	
1.9	-18.5	2423	
2.2	-21.1	2442	
2.5	-23.7	2452	
2.8	-26.3	2457	2470
3.0	-28.8	2468	
3.3	-31.4	2460	
3.6	-34.0	2486	2485
3.9	-36.6	2480	
4.1	-39.2	2476	
4.4	-41.7	2482	
4.7	-44.3	2492	2504
4.9	-46.9	2496	2513
5.2	-49.5	2508	
5.5	-52.1	2530	
5.8	-54.7	2516	
6.0	-57.3	2515	
6.3	-59.9	2503	
I1658 (// to the bar)			
0.5	52.0	2209	
0.8	58.9	2196	
1.1	56.3	2230	2217
1.3	53.7	2243	2250
1.6	51.1	2262	2256
1.9	48.5	2259	2263
2.2	45.9	2256	2259
2.4	43.4	2277	2271
2.7	40.8	2271	2296
3.0	38.2	2290	2303
3.3	35.5	2303	2298
3.5	33.0	2315	
3.8	30.4	2321	
4.1	27.8	2329	
4.3	25.2	2342	2352

X	Y	V(Hα)	V(NII)
4.6	22.7	2336	
4.9	20.1	2348	
5.2	17.5	2348	2345
5.4	14.9	2367	
5.7	12.4	2385	2377
5.9	9.8	2398	2371
6.2	7.2		2382
6.5	4.6	2370	2389
6.8	2.0	2380	2382
7.0	-0.6		2408
7.3	-3.2	2401	
7.6	-5.8	2452	
7.9	-8.4	2470	
8.1	-11.0	2500	
9.5	-23.9	2470	
10.2	-31.7	2526	
10.6	-34.2	2541	
10.9	-36.8	2540	
11.2	-39.4	2507	
11.5	-42.0	2500	
11.7	-44.5	2528	
12.0	-47.1	2525	
12.2	-49.7	2526	2505
12.5	-52.3	2528	2520
12.8	-54.9	2520	2527
I1667 (// to the bar)			
-3.5	47.8		2241
-3.2	45.3		2245
-3.0	42.7		2247
0.2	11.7	2358	
0.5	9.1	2379	
0.8	6.5	2380	
1.0	3.9	2387	
2.4	-9.1	2367	2388
2.7	-11.7	2374	2376
3.0	-14.2	2399	2369

X	Y	V(Hα)	V(NII)
3.2	-16.7	2381	
3.5	-19.4	2394	
3.8	-22.0	2456	
4.1	-24.6	2445	2439
4.3	-27.1	2445	2461
4.6	-29.7	2451	
3.9	-32.3	2456	
4.2	-34.9	2487	
4.4	-37.5	2474	2480
4.7	-40.1	2505	2530
5.0	-42.7	2527	2524
5.2	-45.3	2510	2510
5.5	-47.8	2516	
5.8	-50.4	2490	
I2098			
-63.5	49.6	2215	
-61.4	48.0	2227	
-59.4	46.4	2227	
-57.4	44.6	2235	
-55.3	43.2	2224	
-49.2	38.4	2225	
-47.1	36.8	2247	
-45.1	35.2	2266	
-43.0	33.6	2265	
-41.0	32.0	2240	
-38.9	30.4	2233	
-36.9	28.3	2251	
-34.8	27.2		2248
-32.8	25.5	2252	2289
-30.7	24.0	2258	2266
-28.7	22.4	2275	2281
-26.6	20.8		2290
-20.5	16.0		2292
-18.4	14.4		2297
-16.4	12.8		2322
-12.3	9.6		2326
-10.2	8.0		2319
-8.2	6.4		2317
-6.1	4.8		2323
-4.1	3.2	2335	2333

X	Y	V(Hα)	V(NII)
-2.0	1.6	2375	
0.0	0.0		2385
2.0	-1.6	2460	
8.2	-6.4	2487	
10.2	-8.0	2504	
12.3	-9.6	2470	
14.3	-11.2	2457	
16.4	-12.8	2475	
18.4	-14.4	2485	
24.6	-19.2	2437	
26.6	-20.8	2473	
28.7	-22.4	2482	
30.7	-24.0	2475	
32.8	-25.6	2471	
34.8	-27.2	2452	
38.9	-30.4	2460	
41.0	-32.0	2495	
43.0	-33.5	2492	
45.1	-35.2	2478	
47.1	-36.8	2481	
49.2	-38.4	2496	
51.2	-40.0	2495	
53.2	-41.6	2465	
63.5	-49.6	2500	
65.6	-51.2	2514	
67.6	-52.8	2490	
69.7	-54.4	2501	2501
71.7	-56.0	2500	
73.8	-57.6	2507	2526
75.8	-59.2	2506	2505
77.9	-60.8	2507	
81.9	-64.0	2522	2532
84.0	-65.6	2520	2517
86.1	-67.2	2529	
I2101			
-69.9	6.1	2249	
-67.3	5.9	2245	
-64.7	5.7	2267	
-62.2	5.4	2251	
-59.6	5.2	2241	

X	Y	V(Hα)	V(NII)
-57.0	5.0	2226	
-54.4	4.8	2228	
-51.8	4.5	2280	
-49.2	4.3	2314	
-46.6	4.1	2300	
-44.0	3.8	2313	
-41.4	3.6	2340	
-38.8	3.4	2293	
-36.3	3.2	2270	
-33.7	2.9	2248	
-18.1	1.6	2326	
-7.8	0.7		2332
-5.2	0.5		2335
-2.6	0.2		2343
0.0	0.0	2382	
2.6	-0.2	2384	
7.8	-0.7	2398	
10.4	-0.9	2401	
12.9	-1.1	2408	
20.7	-1.8	2412	
41.4	-3.6	2367	
51.8	-4.5	2384	
54.4	-4.8	2385	
57.0	-5.0	2403	
54.7	-5.7	2429	
67.3	-5.9	2416	
70.0	-6.1	2380	
72.5	-6.3	2381	
75.1	-6.6	2398	
77.7	-6.8	2410	
80.3	-7.0	2440	
82.9	-7.3	2452	
85.5	-7.5	2422	
88.1	-7.7	2426	

Note to tables IVa, b, c.

X, Y : coordinates in arcsecond in the galaxy plane. Axis X in the West direction, Y in the North. The origin is the center of outer isophotes. V (Hα), V (N II) radial velocities in km s^{-1} measured from Hα et [N II] lines.

a)

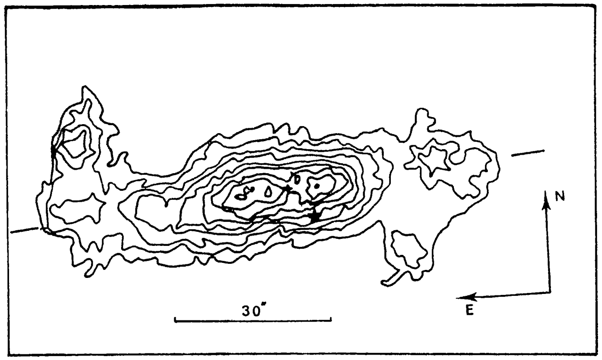

Central part
Outer isophote μ=22.25, step: 0.25 mag arcsec^{-2}

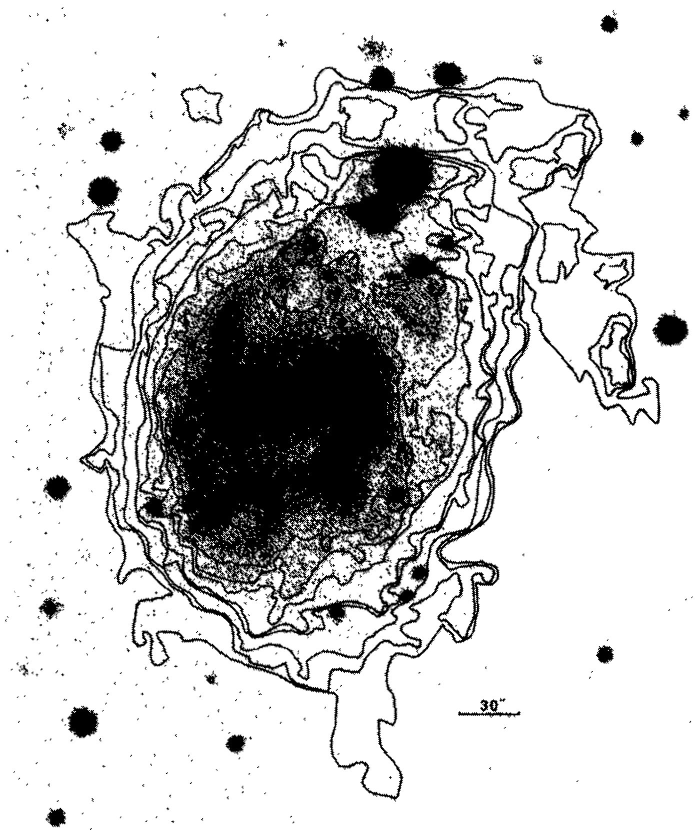

Outer isophote μ=27.00, step: 0.50 mag arcsec^{-2}

b)

Outer isophote μ=26.10, step: 0.50 mag arcsec^{-2}

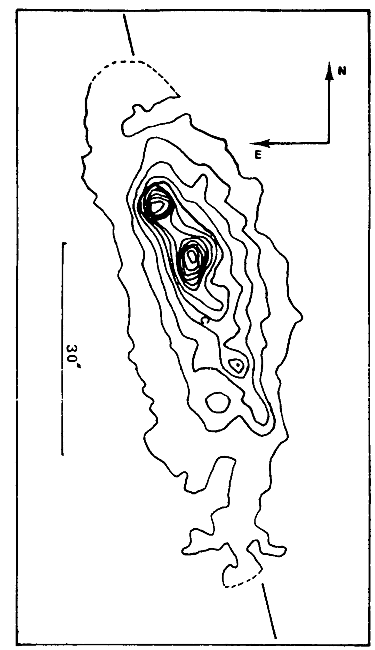

Central part
Outer isophote μ=21.60 I=1.00
step: ΔI=0.40

FIGURE 1b.

FIGURES 1a-c. — a) *B* isophotal map of NGC 7741. b) *B* isophotal map of NGC 3359.
c) *B* isophotal map of NGC 7479.

c)

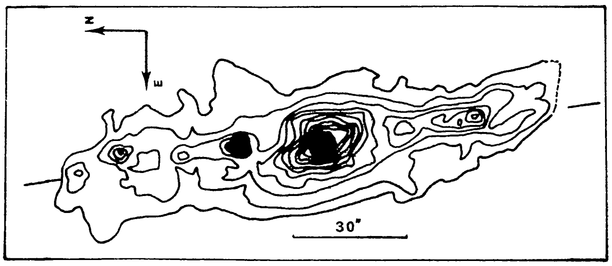

Central part
Outer isophote μ=22;37
I=0.46, step:ΔI=0.25

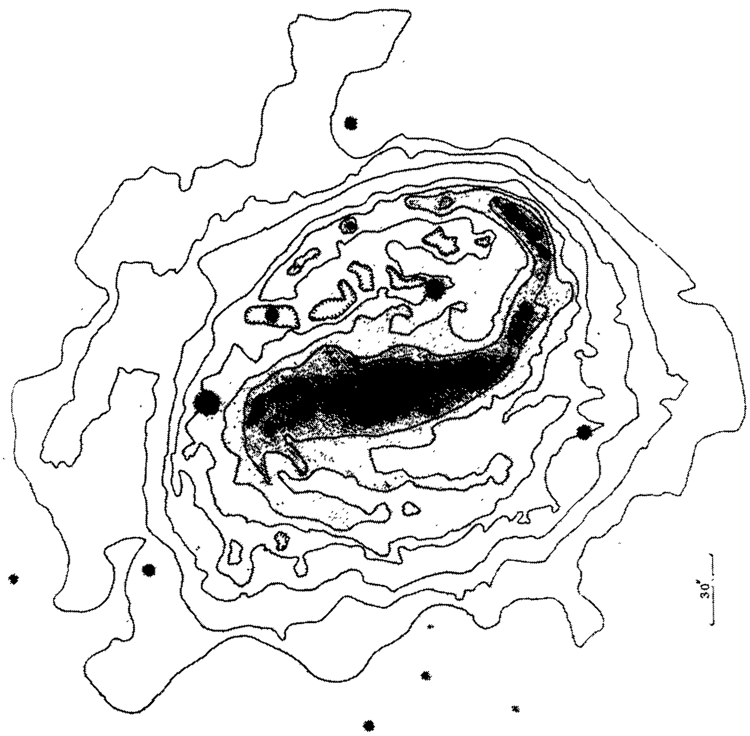

Outer isophote μ = 25.53 , step: 0.50 mag arcsec^{-2}

FIGURE 1 *(continued)*.

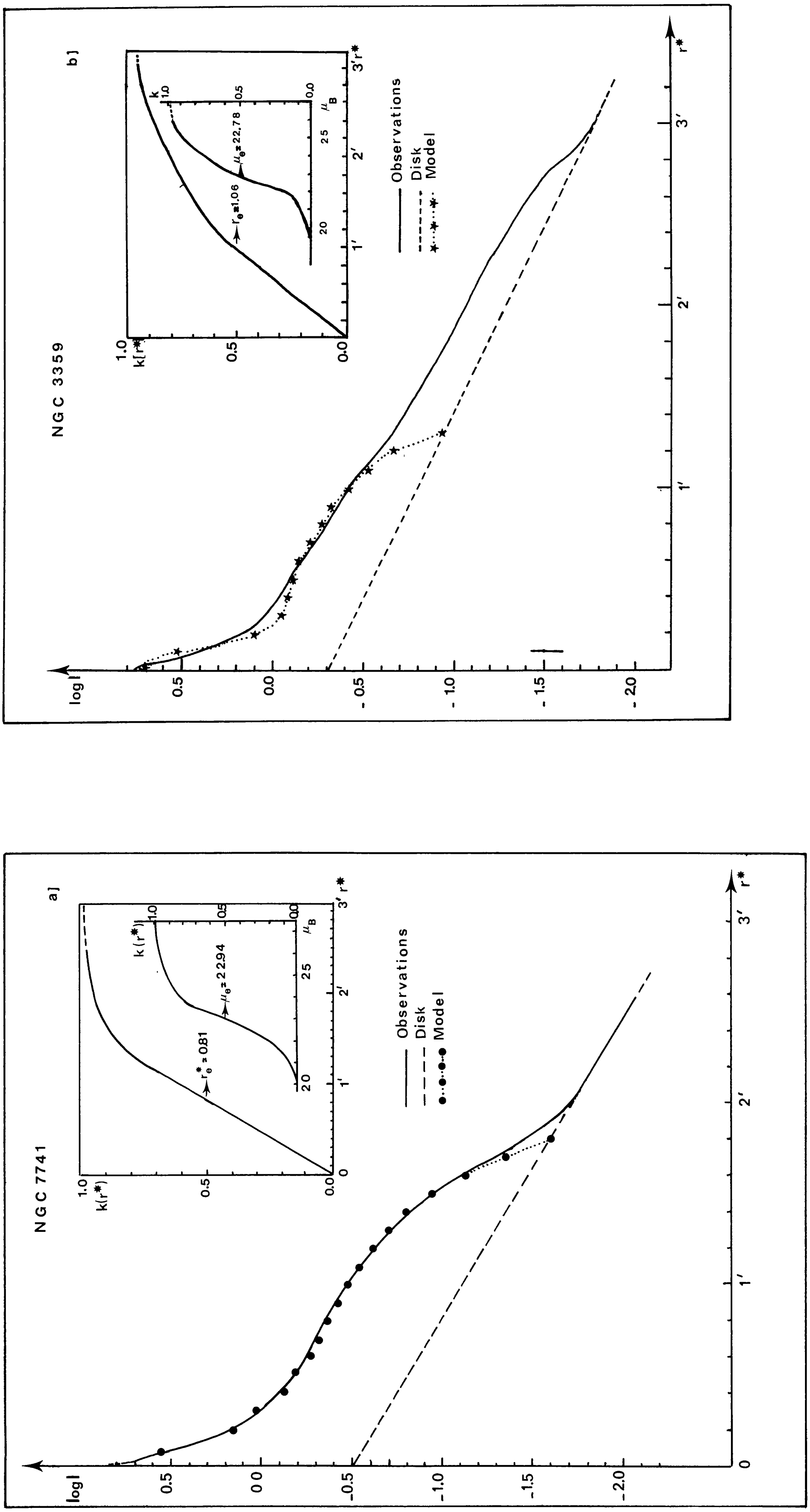

FIGURES 2a-c. — Equivalent mean luminosity profile and relative integrated luminosity curve.

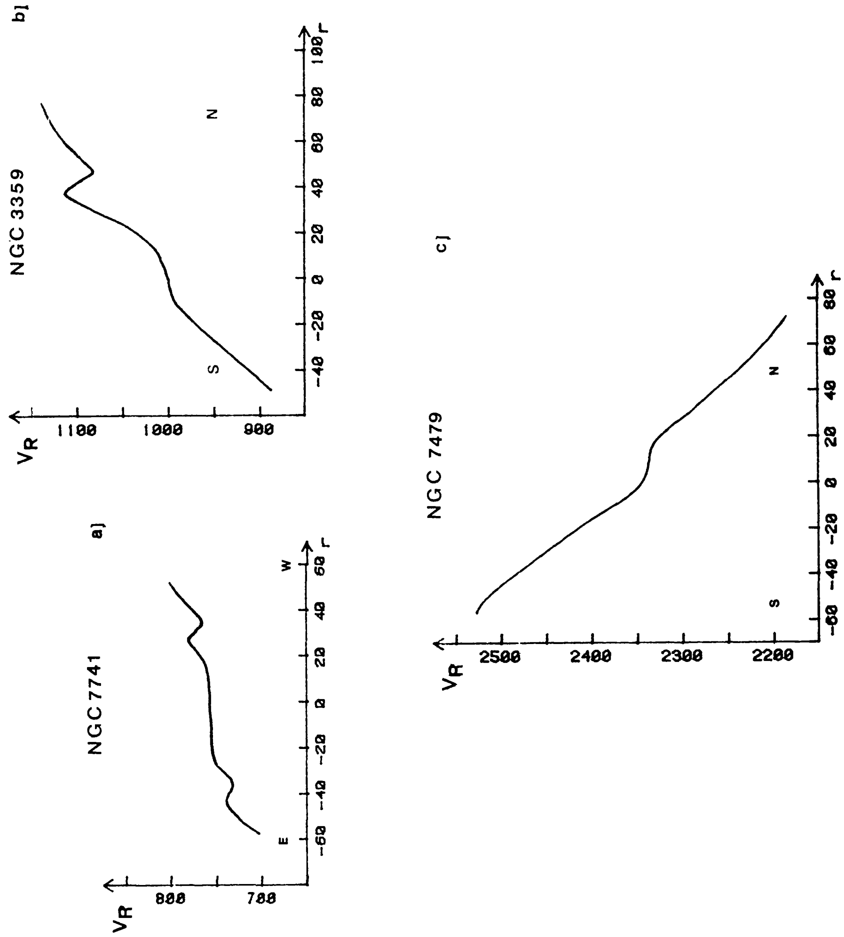

FIGURES 3a-c. — Mean radial velocity observed along the bar.

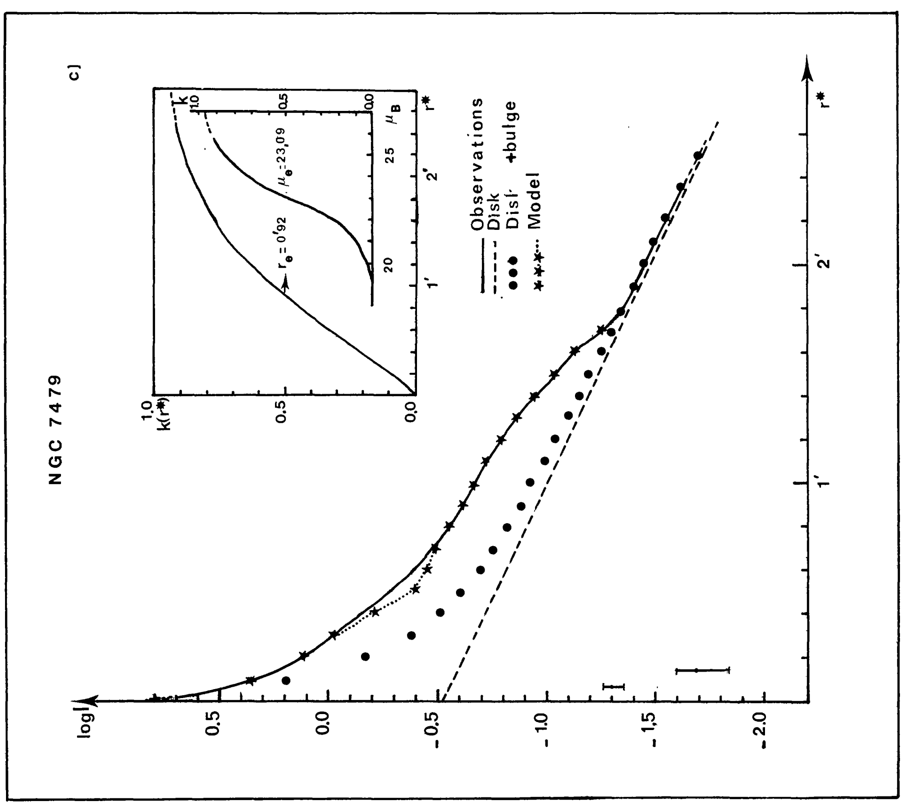

FIGURE 2 *(continued)*.

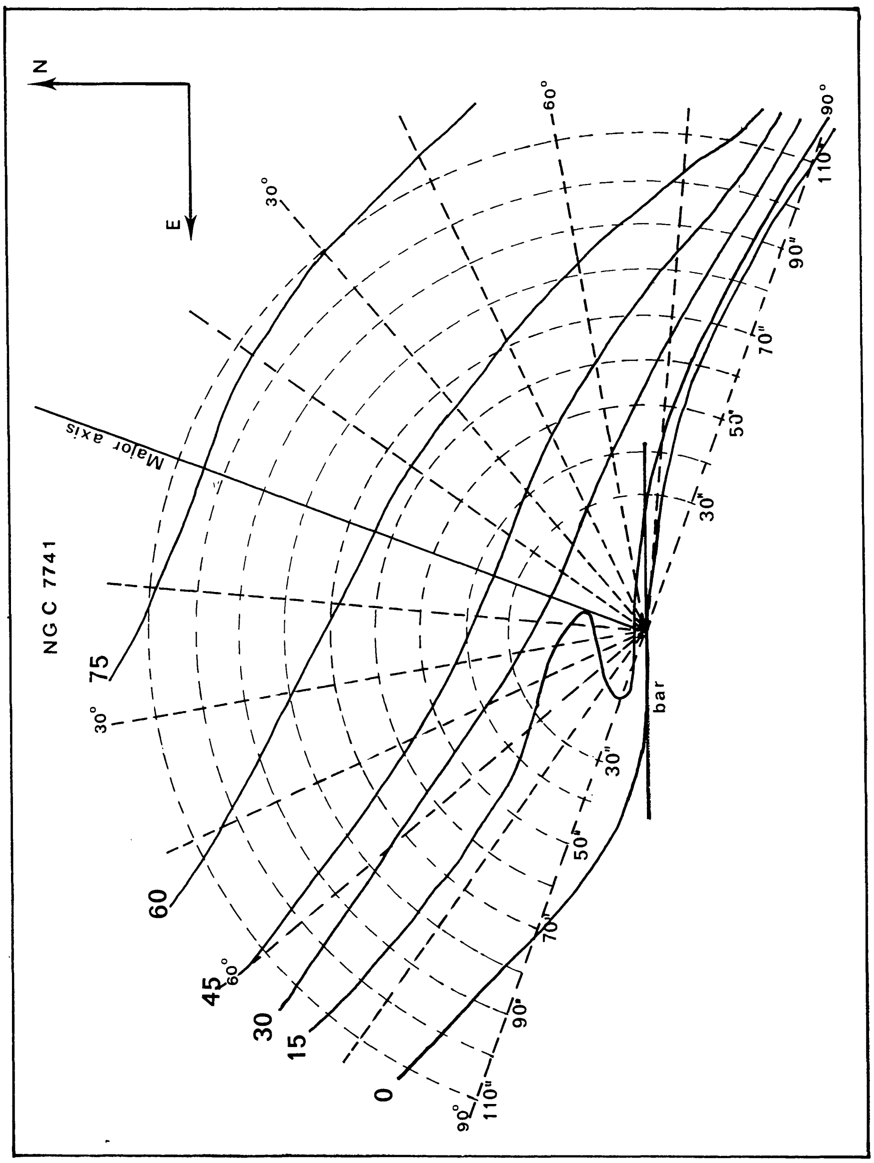

FIGURE 4. — Isovelocities in the galaxy plane in km s^{-1}.

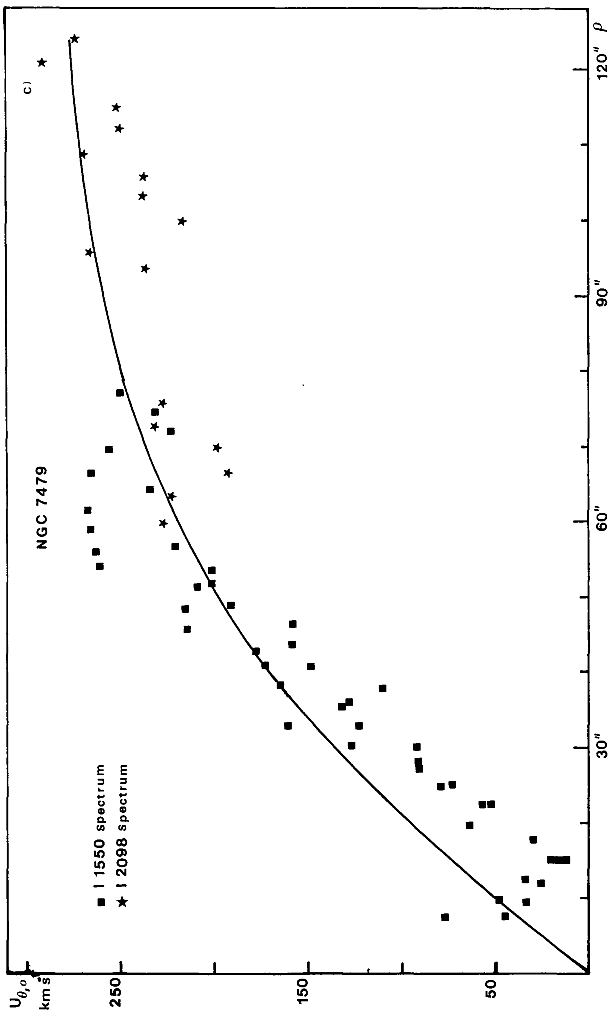

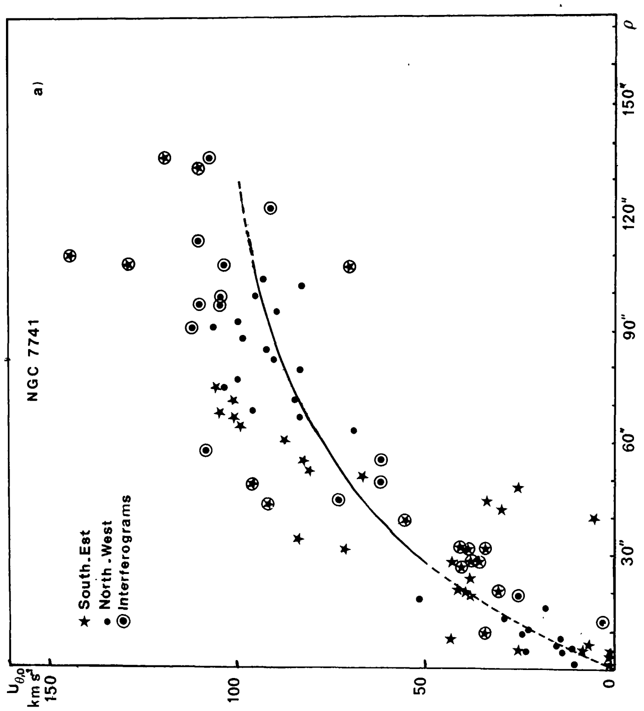

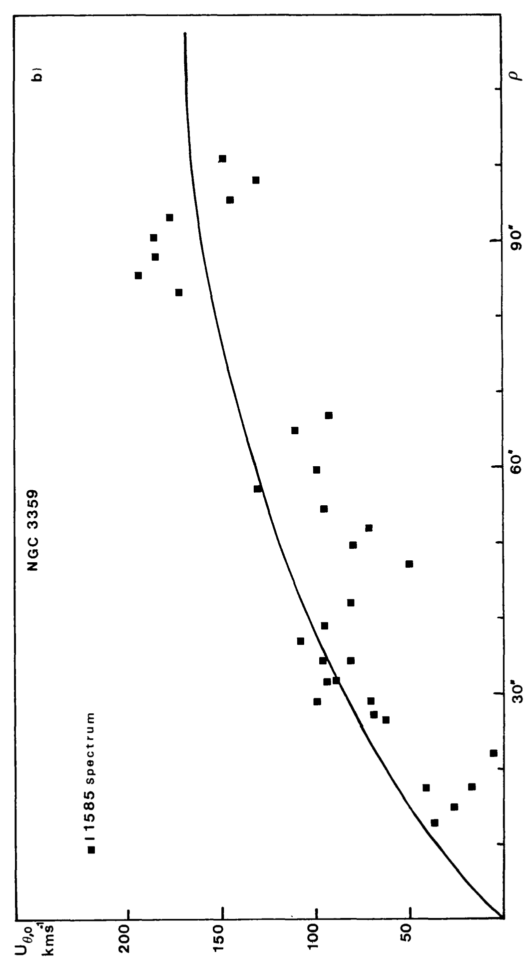

FIGURES 5a-c. — Axisymmetric rotation curve in the galaxy plane.

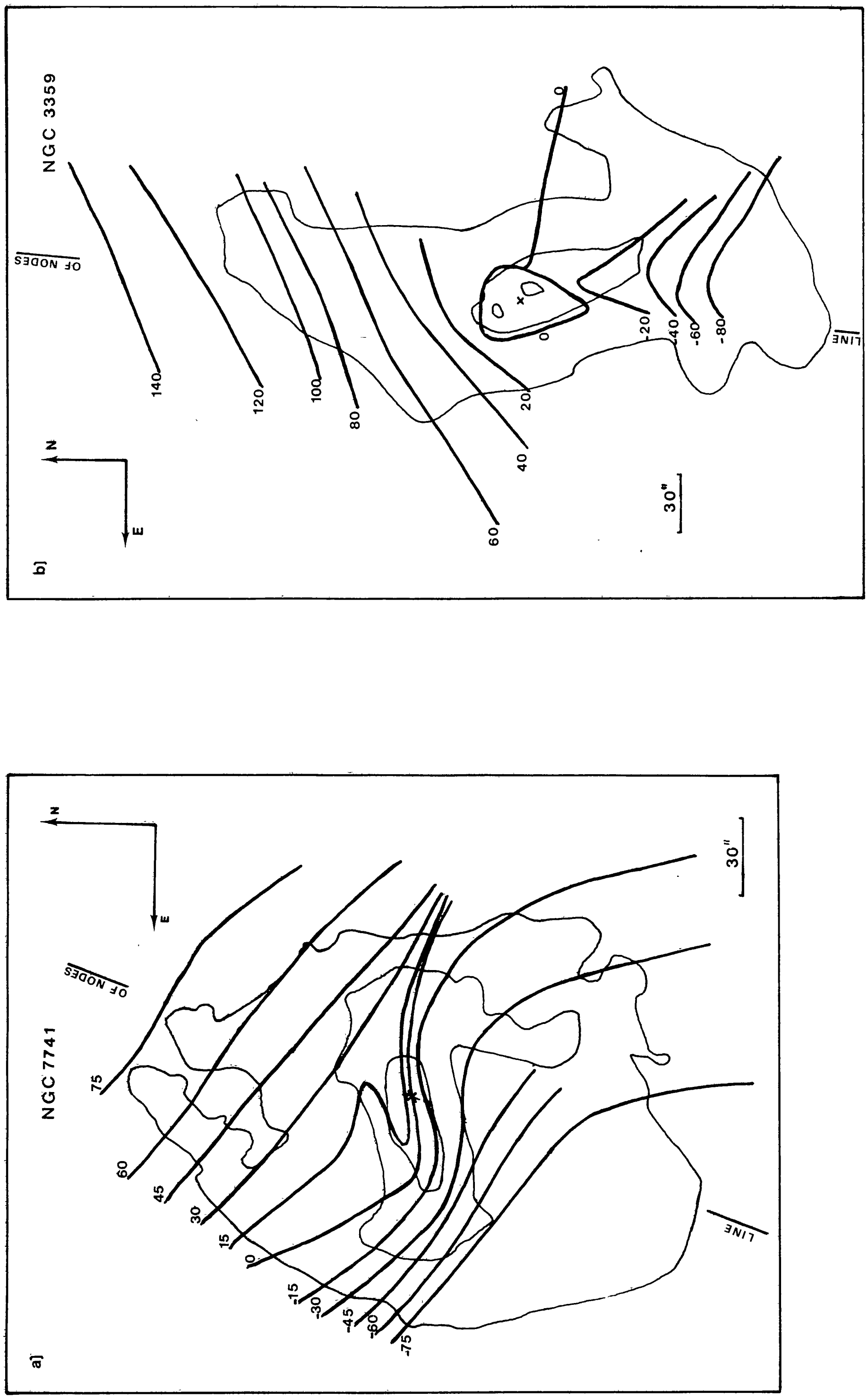

FIGURES 6a-c. — Isoradial velocities in km s^{-1} superposed on some blue isophotes (sky plane).

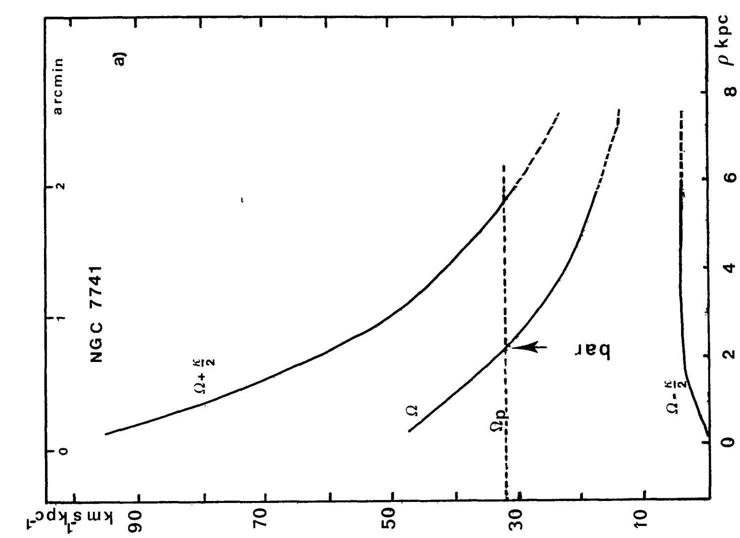

FIGURE 7a-c. — Resonance curves.

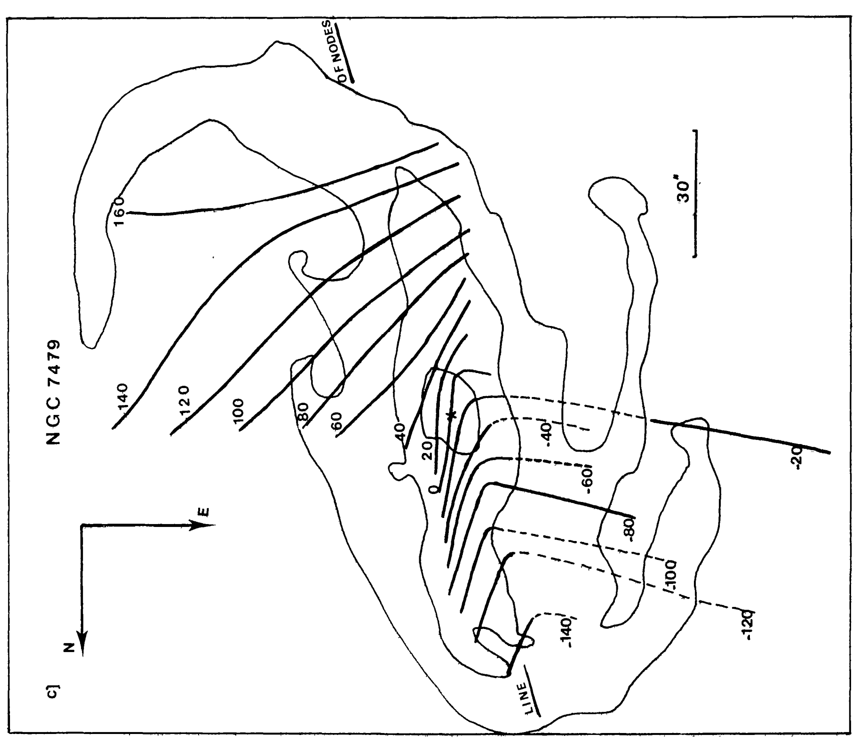

FIGURE 6 (continued).

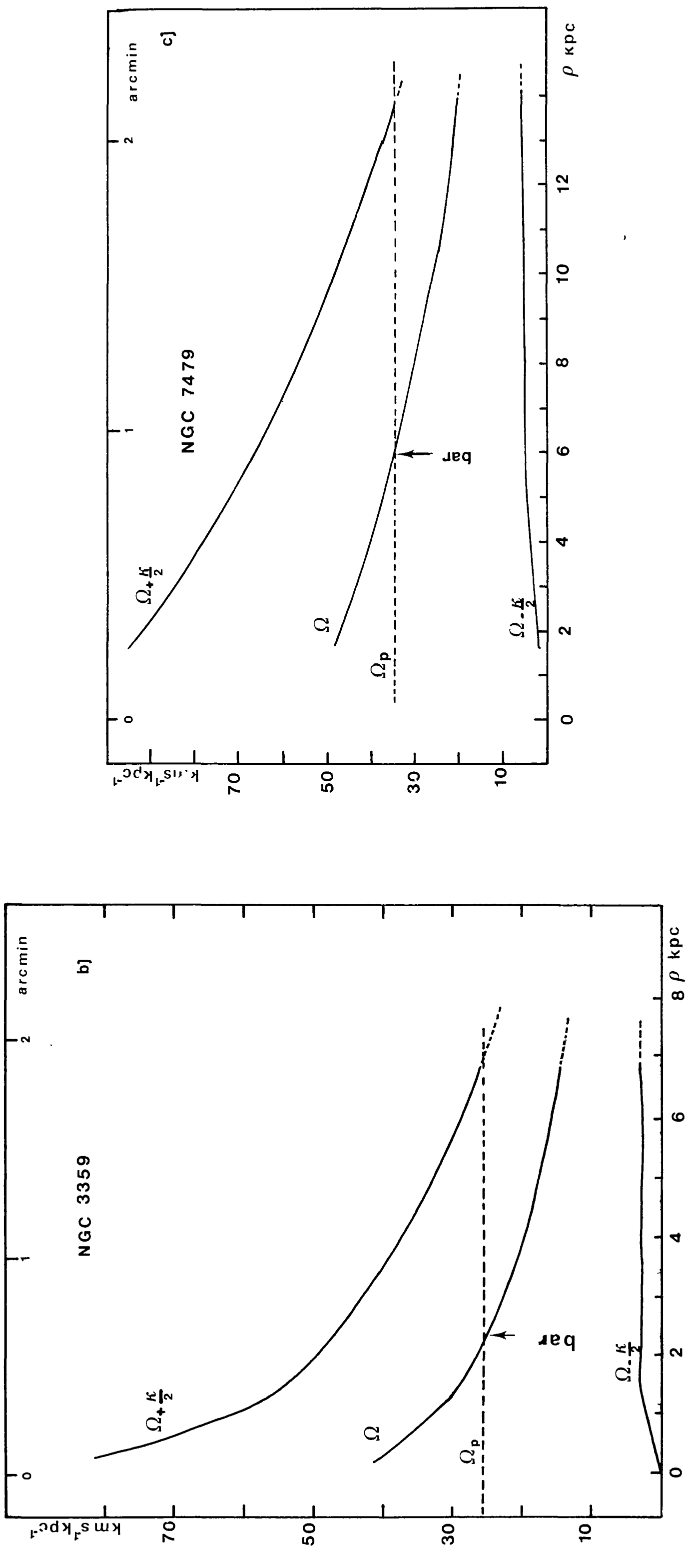

FIGURE 7 (*continued*).